Atomistic simulations of dislocation/precipitation interactions in Mg-Al alloys and implications for precipitation hardening

Amitava Moitra[1], Javier LLorca[1,2,*]

[1] *IMDEA Materials Institute*
C/ Eric Kandel 2, 28906 - Getafe, Madrid

[2] *Department of Materials Science, Polytechnic University of Madrid*
E. T. S. de Ingenieros de Caminos. 28040 - Madrid, Spain.

Abstract

Atomistic simulations were carried out to analyze the interaction between $< a >$ basal dislocations and precipitates in Mg-Al alloys and the associated strengthening mechanisms. It was found that β-$Mg_{17}Al_{12}$ precipitates were sheared by either edge or screw basal dislocations regardless of the precipitate orientation, applied stress and temperature. The critical resolved shear stress to cut the precipitates increased with precipitate size and was larger than the theoretical Orowan strength at 0K for most precipitate sizes but dislocation loops around the precipitate were never observed. Moreover, molecular dynamics simulations showed that the activation free energy for precipitate shearing was very low and, thus, the stress necessary to shear the precipitates decreased rapidly in the presence of thermal activation. All together, these atomistic simulations provide new insights in the limited strengthening provided by β-$Mg_{17}Al_{12}$ precipitates in Mg-Al alloys.

Keywords: Atomistic simulations, Mg-Al alloys, dislocation-precipitate interactions, precipitation hardening

*Corresponding author

1. Introduction

Metallic materials stand for the structural materials *per excellence* as a result of their outstanding stiffness, strength and toughness. In particular, the combination of strength and toughness is the result of plastic deformation mediated by the glide of dislocations, which is a very efficient mechanism to dissipate energy before fracture. However, the stress necessary to move dislocations in pure metals is very low and the design metallic alloys with higher resistance to dislocation glide is one of the main goals of physical metallurgy. Besides the strain hardening due to dislocation-to-dislocation interactions and to the interaction of dislocations with grain boundaries, solute and precipitation hardening are the main strengthening mechanisms in metallic alloys. Among them, the strengthening provided by precipitates is much higher than that obtained by solute hardening [1]. Moreover, the energy barrier induced by the presence of precipitates is much higher and precipitate hardening is still effective at high temperatures while solute-hardening decreases rapidly with temperature [1, 2].

Al-Cu and Ni-based superalloys with an FCC lattice are excellent examples of the ability of precipitates to increase the flow strength of metallic materials up to temperatures that are determined by the thermodynamic stability of the precipitates. However, similar success has not been achieved in Mg alloys [3], whose HCP lattice presents fundamental differences in the deformation mechanisms with respect to FCC alloys [4, 5, 6]. In particular, plastic deformation of Mg and Mg alloys takes place by dislocation glide in three different slips systems (basal, prismatic and pyramidal slip) as well as by tension twinning as opposed to only one slip system in FCC metals. The large differences in the critical resolved shear stresses to activate plastic slip in the different systems in Mg as well as the polarity of twinning (which only takes place when the c axis of the HCP lattice is extended), lead to the plastic anisotropy of Mg alloys, that has very negative effects on the ductility [7, 8].

Basal slip is the softest slip system in Mg and Mg alloys, and increasing the critical resolved shear stress for dislocation slip in this system is particularly important because the yield strength is improved and the plastic anisotropy is reduced [7]. Precipitation hardening has been used to this purpose but the contribution of precipitates to strengthen basal slip has been limited [9, 10, 11, 12]. Continuum models, based on the Orowan mechanism,

have been applied to ascertain the influence of the precipitate size, shape, orientation and spatial distribution on the critical resolved shear stress on the different slip systems in Mg [13, 6, 12] . Although these models were able to rationalize some of the experimental trends, it should be noticed that the Orowan model assumes a very simplistic approach for the dislocation/precipitate interaction: the precipitates are rigid obstacles overcome by dislocations by the formation of an Orowan loop. Moreover, evidence of precipitate shearing by basal dislocations has been recently presented in micropillar compression tests in Mg - 5 wt.% Zn alloys [14] (and not the formation of Orowan loops) and thus the actual deformation mechanisms are not well established. Thus, simulations at smaller length scales (either using dislocation dynamics [15, 16, 17] or molecular dynamics [18, 19, 20, 21, 16]) are required to get a better understanding of the dislocation/precipitate interactions and to develop more accurate models.

In this investigation, molecular statics and dynamics simulations were carried out to assess the strengthening effect and the interaction between basal dislocations and precipitates in Mg-Al alloys. Mg-Al alloys are well-known among Mg alloys for their excellent castability and corrosion resistance and can be strengthened by means of β-$Mg_{17}Al_{12}$ intermetallic precipitates [22, 3]. Molecular statics simulations were carried out to determine the Critical Resolved Shear Stress (CRSS) and the mechanisms of dislocation/precipitate interaction as a function of the dislocation type, precipitate size and orientation as well as after successive shearing of the precipitate by dislocations. Molecular dynamics simulations were then carried out in selected cases to ascertain the activation free energy, which was compared with the data on precipitate-hardened Al-Cu alloys.

2. Background on precipitate-strengthened Mg-Al alloys

Precipitation of β-$Mg_{17}Al_{12}$ intermetallic occurs in Mg-Al alloys when the cooling rate of the casting is sufficiently slow or by means of ageing treatments after casting [3]. The β-phase $Mg_{17}Al_{12}$ has a complex body-center cubic structure with a lattice parameter of 1.056 nm within the space group *I-43m*. The unit cell includes 34 Mg atoms and 24 Al atoms [23]. β precipitates grow in the matrix along preferred orientations. The most common orientation relationship (OR) for lath-shaped or lozenge-shaped precipitates is $[0001]_{Mg} \parallel [110]_{\beta}$ [24, 4, 25]. Precipitates with this OR are parallel to the basal

plane of Mg, i.e the habit plane is $(0001)_{Mg}$. Rod-shaped precipitates with OR $[0001]_{Mg} \parallel [111]_{\beta}$ have also been reported [24], although they are less common. Precipitates following this OR lie on the prism plane of the Mg matrix with habit plane $(1\bar{1}00)_{Mg}$.

The solid solubility of Al in α-Mg at the eutectic temperature is 11.8 at. % and decreases up to 3.3 at. % at 200°C. The equilibrium volume fraction of β $Mg_{17}Al_{12}$ precipitates can reach 11.4% when the alloy is aged at 200°C [26]. Although this fraction is very large, the age hardening response of Mg-Al alloys is not as good as it could be desired. It has been argued that the limited precipitation hardening of Mg-Al alloys occurs because most of the precipitates present the OR $[0001]_{Mg} \parallel [110]_{\beta}$ and lay parallel to the basal plane, which is the least efficient to block basal slip [9]. It was also suggested [26] that the precipitate distribution is relative coarse because of the high diffusion rate of Al atoms in the Mg matrix [27]. Finally, it was proposed – based on the Orowan model – that rod-shaped precipitates with OR $[0001]_{Mg} \parallel [111]_{\beta}$ are more efficient than plate-shaped ones to increase the CRSS for basal $< a >$ slip because they intersect a larger number of basal planes for a given precipitate volume fraction [23, 9, 13, 28, 12]. Nevertheless, molecular dynamics simulations of the interaction of basal and prismatic edge dislocations with β precipitates did not show any evidence of the formation of Orowan loops [29, 21]. Thus, the details of the dislocation/precipitate interaction in these alloys as well as the strengthening provided as a function of dislocation type, precipitate size and orientation are not known.

3. Method and Model development

3.1. Interatomic potential

Atomistic simulations of the interaction of $< a >$ basal dislocations with $Mg_{17}Al_{12}$ precipitates were carried out using the open-source parallel molecular dynamics code LAMMPS [30]. There are four interatomic potentials currently available in order to model the Mg-Al system: Liu's Embedded Atom Method (EAM) (alloy type) [31], Mendelev's EAM (Finnis-Sinclair type) [32], Jelinek's Modified Embedded Atom Method (MEAM) [33] and Kim's 2NN MEAM [34]. Out of these four potentials, Jelinek's MEAM potential predicts a positive formation energy of 49 meV/atom for the $Mg_{17}Al_{12}$ phase, as compared to -39 meV/atom obtained from density functional theory (DFT) calculations [33].

Potential	Stacking fault energy (mJ/m^2)	Stacking fault width (nm)	Peierls stress (MPa)
Liu [31]	54.9	1.4	12.0
Mendelev [32]	35	2.01	10.6
Kim [34]	30	2.66	11.3
DFT [33]	37		

Table 1: Properties of $< a >$ edge basal dislocations in Mg for different Mg-Al interatomic potentials. The DFT predictions for the stacking fault energy are also shown for comparison [33]

Molecular statics simulations of the structure and the Peierls stress of $< a >$ edge basal dislocations in Mg were carried out with the three other potentials. The magnitudes of the of the stacking fault energy, stacking fault width and the Peierls stress for $< a >$ basal dislocations are shown in Table 1 together with the DFT predictions for the stacking fault energy. Both Mendelev and Kim potentials provide stacking fault energies very similar to the DFT results, while the Peierls stress of the three potentials for <a> basal dislocations is very close and higher than the experimental values [35]. Preliminary molecular statics simulations were also carried out to analyze the dislocation/precipitate interaction in Mg-Al alloys with the three potentials. Dislocations initially sheared the precipitates in all cases but a spurious jog developed when the dislocation was cutting the precipitate in the case of Liu and Kim potentials. The dislocation inside the precipitate climbed to the precipitate/matrix interface and slipped along the interface without shearing the precipitate. This behavior was already reported [21] but we found the length of the jog increased with the height (perpendicular to the basal slip plane) of the precipitate. Thus, very large jogs (of several nm in length) developed, which are merely artifacts resulting from the atomic potentials. This behaviour was not found in the case of the Mendelev potential, which was selected for the present simulations.

3.2. Geometry, boundary conditions and loading

The simulation box (Fig. 1) was parallelepipedic and the X, Y and Z axes were parallel to the $[11\bar{2}0]$, $[10\bar{1}0]$ and [0001] orientations of the HCP Mg lattice. The dimensions of the box were $48 \times 33 \times 21$ nm^3 in the case of edge dislocations and $54 \times 33 \times 21$ nm^3 in the case of screw dislocations. They were chosen following the results of Szajewski and Curtin [36] to minimize

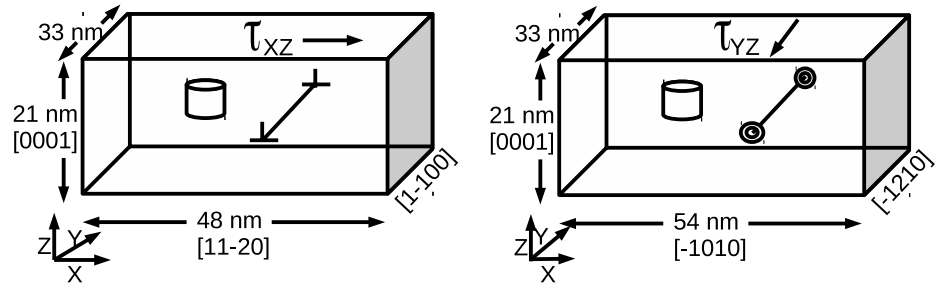

Figure 1: Simulation cells for atomistic simulations of <a> basal dislocation/precipitate interactions. The precipitate has a disk shape and is parallel to the (0001) plane. (a) Edge dislocation. (b) Screw dislocation. The crystallographic orientation and the cell dimensions are indicated in the figure. Shear stresses were applied to the atoms on the top surface while the atoms at bottom surface were fixed.

the image stresses for the number of atoms (≈1.8 millions) in the simulation box. A dislocation (edge or screw) and a $Mg_{17}Al_{12}$ cylindrical precipitate with a given size and orientation were introduced in the simulation box (Fig. 1). The dislocation line was always parallel to the Y axis. The atom positions corresponding to the HCP lattice of Mg were first generated in desired crystallographic orientations. In the case of the edge dislocation, $X \parallel [11\bar{2}0]$, $Y \parallel [1\bar{1}00]$ and $Z \parallel [0001]$ (Fig. 1a). The edge dislocation was included by deleting a half-plane of atoms on the $(11\bar{2}0)$ plane using ATOMSK [37]. In the case of the screw dislocation, the crystallographic orientation of the simulation box was $X \parallel [\bar{1}010]$, $Y \parallel [\bar{1}210]$ and $Z \parallel [0001]$ (Fig. 1b). ATOMSK was also used to introduce a screw dislocation by applying a displacement in the plane normal to the dislocation line to all the atoms assuming isotropic elasticity.

After either the edge or screw dislocation was introduced, periodic boundary conditions were applied to the cell surfaces and the configuration was relaxed using the conjugate gradient algorithm. The dislocation was dissociated into two Shockley partials according to $1/3[11\bar{2}0] \rightarrow 1/3[10\bar{1}0] + 1/3[01\bar{1}0]$, which bound the stacking fault. The width of the edge (screw) dislocation core was reduced to almost 1.9 nm (1.6 nm), which is close to previous atomistic results and experimental observations [38].

The precipitates have a disk shape with 3 nm in height. A void of these dimensions was created in the cell and the atom positions of the β-$Mg_{17}Al_{12}$

precipitates following the ORs $[0001]_{Mg} \parallel [110]_{\beta}$ or $[0001]_{Mg} \parallel [111]_{\beta}$ were generated and introduced into the void. The basal plane of the Mg lattice was parallel to the disk and the dislocation line was aligned with the midsection of the precipitate disk. The whole simulation cell was relaxed again using the conjugate gradient algorithm and the equilibrium distance between the edge of the precipitate and the dislocation line was approximately 2 nm.

The periodic array of dislocations model [39] was used to analyze the dislocation/precipitate interactions. To this end, periodic boundary conditions were applied along the glide direction X and the dislocation line Y. They were adapted from previous studies to reduce the non-glide stress components that can affect the dislocation motion [40, 41, 38]. The position of the six layers of atoms at the bottom surface remained fixed during the simulations while six layers of atoms at the top surface were fixed along their normal direction Z and constrained to two-dimensional displacements in the XY plane. Incremental displacements of 0.02 nm were applied to the atoms at the top surface along the X (Y) axis in order to move the edge (screw) dislocation. The conjugate gradient method was used to minimize the energy of the system after each incremental displacement. The energy minimization algorithm was modified by restricting the maximum atom movement to 0.02 nm in a single line search in any dimension to increase the resolution of the simulations.

Molecular dynamics (MD) simulations were conducted to ascertain the influence of the temperature on the shearing mechanisms and also to gain insights on the energy barriers associated with this process. MD simulations were carried out using NPT ensemble with Mendelev's EAM potential. The simulation boxes were identical to the ones in Fig. 1 and contained an edge or screw dislocation and a disc-shaped precipitate of 8 nm in diameter and 3 nm in height. A fixed shear stress and fixed temperature were maintained using the Parrinello-Rahman algorithm [42] with a damping parameter of 1 ps. Periodic boundary conditions were applied along X and Y directions, while six layers of atoms at the top surface were fixed along their normal direction Z and constrained to two-dimensional displacements in the XY plane. Simulations were carried out with both an edge and a screw dislocation at 150K and 350K for precipitates with both ORs.

The shear stress τ_{xz} (τ_{yz}) induced by the incremental displacement eventually led to the edge (screw) dislocation movement along the X axis, and

the dislocation glide was hindered by the precipitate. The volume-averaged stress tensor $\sigma_{\alpha\beta}$ was calculated by using Virial definition without the kinetic energy contribution according to [43]

$$\sigma_{\alpha\beta} = \frac{1}{V} \sum_{i}^{N^*} \sum_{j(\neq i)}^{N} f_{\alpha}^{ij} r_{\beta}^{ij} \tag{1}$$

where f_{α}^{ij} is the force vector between atoms i and j in the direction α, r_{β} the distance vector in direction β, N the number of neighbour atoms for atom i, N^* the total number of atoms, and V the simulation cell volume. The common neighbour analysis (CNA) [44, 45] was used to identify the atomic structure. Visualization of the atomic configurations were obtained using the Open Visualization Tool (OVITO) [46].

4. Results and discussion

The atomistic model presented above is used to analyze the basal dislocation-precipitate interaction in the athermal limit as well as the CRSS necessary to overcome the precipitate for the two precipitate ORs. The $Mg_{17}Al_{12}$ precipitates were approximated by circular disks [13, 6] with a diameter in the range 2 nm to 10 nm and a constant height of 3 nm. Interaction of both edge and screw dislocations with the precipitates was ascertained for each precipitate orientation and diameter.

4.1. Interaction mechanisms

The interaction of a basal edge dislocation with a precipitate with the OR $[0001]_{Mg} \parallel [110]_{\beta}$ is shown in Fig. 2 and Fig. 3 for precipitates of 2 nm and 8 nm in diameter, respectively. In both cases, the X axis (horizontal) was parallel to the [111] direction in the precipitate. All the HCP atoms (Mg-matrix), determined using common-neighbours analysis, were removed from the plot, and only the partial dislocations, stacking fault, and the precipitate are shown. As the dissociated dislocation approaches the precipitate, the leading partial (LP) is attracted, enters and shears the precipitate, Figs. 2b) and 3b). Afterwards, the trailing partial (TP) is also attracted and shears the precipitate, becoming closer to the LP, Figs. 2c) and 3c). The width of the dislocation stacking fault in the Mg becomes narrower around the precipitate

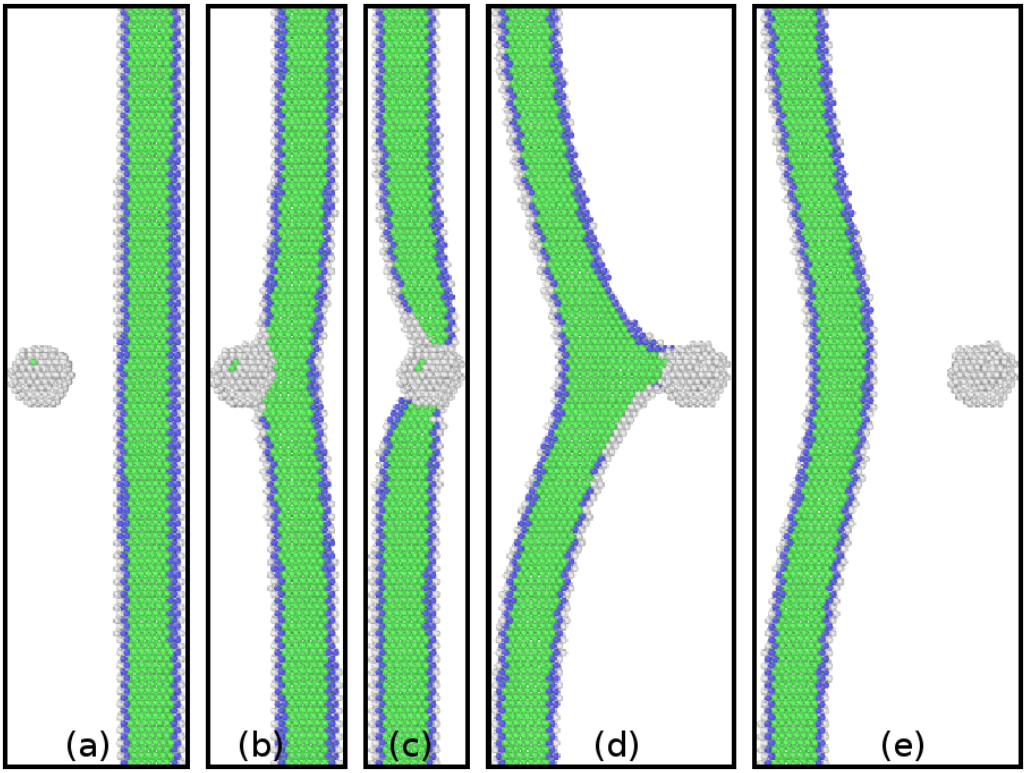

Figure 2: Progressive shearing of a $Mg_{17}Al_{12}$ precipitate of 2 nm in diameter by an edge basal dislocation. The OR was $[0001]_{Mg} \parallel [110]_{\beta}$ and the X axis (horizontal) was parallel to the [111] direction in the precipitate. The Z axis is perpendicular to the figure. Atoms in HCP positions are not shown. Green atoms are in FCC positions while blue atoms are in BCC positions. Precipitate and atoms in unknown positions are grey.

when both the LP and TL are within the precipitate and the shape of the LP and TP indicates that the precipitate is an obstacle to the dislocation motion. Finally, the LP overcomes the precipitate but the TP is pinned by the precipitate and it is only able to overcome the precipitate when the TP lines are parallel to the Burgers vector, Figs. 2d) and 3d). Thereafter, the TPs are also combined, and the full edge dislocation bypasses the precipitate, Figs. 2e) and 3e). This mechanism was the same in the whole range of precipitate diameters analyzed (2 to 10 nm) and for precipitates with OR $[0001]_{Mg} \parallel [110]_{\beta}$ and $[0001]_{Mg} \parallel [111]_{\beta}$. The latter are not shown for the sake of brevity.

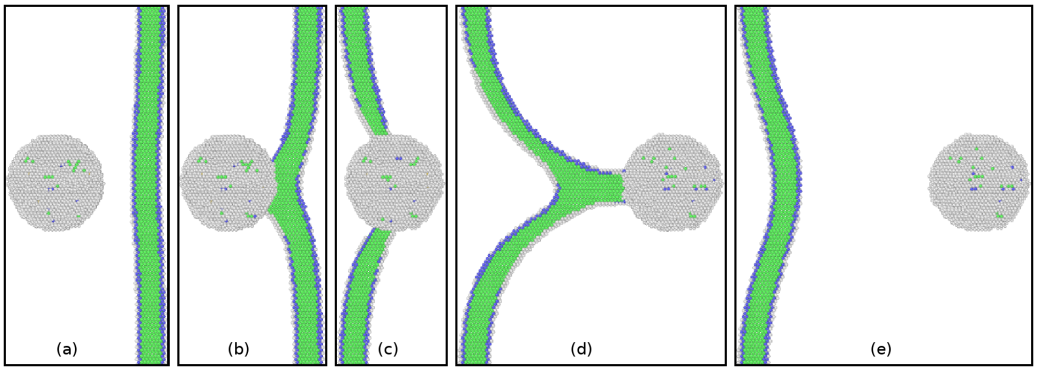

Figure 3: Progressive shearing of a $Mg_{17}Al_{12}$ precipitate of 8 nm in diameter by an edge basal dislocation. The OR was $[0001]_{Mg} \parallel [110]_{\beta}$ and the X axis (horizontal) was parallel to the [111] direction in the precipitate. The Z axis is perpendicular to the figure. Atoms in HCP positions are not shown. Green atoms are in FCC positions while blue atoms are in BCC positions. Precipitate and atoms in unknown positions are grey.

The dislocation/precipitate interactions in the case of a screw dislocation and precipitates with the OR $[0001]_{Mg} \parallel [110]_{\beta}$ are shown in Fig. 4 and Fig. 5 for precipitates of 2 nm and 8 nm in diameter, respectively. In both cases, the X axis (horizontal) was parallel to the [111] direction in the precipitate. The dissociated screw dislocation (with a narrower staking fault, as compared to the edge dislocation) also shears the precipitate and the mechanisms are very similar to those observed in the case of edge dislocations. The TP partial is also pinned during shearing, providing most of the drag for the dislocation motion. Moreover, similar mechanisms were observed in the precipitates with OR $[0001]_{Mg} \parallel [111]_{\beta}$ and they are not shown for sake of brevity.

A more detailed analysis of the dislocation/precipitate interaction was carried out to understand the precipitate plane through which the dislocation shears the precipitate. It was found that the precipitate was sheared through a plane containing Al and Mg atoms in the case of screw dislocations, and in most cases for edge dislocations, regardless of the precipitate size and OR. The analysis of the crystal structure of the $Mg_{17}Al_{12}$ precipitate (Fig. 6) shows that there are three types of {110} and {111} planes in the precipitate containing either Al atoms, Mg atoms or both types of atoms. Although the plastic deformation mechanisms in $Mg_{17}Al_{12}$ are unknown, recent calculations of the generalized stacking fault energy using atomistics have pre-

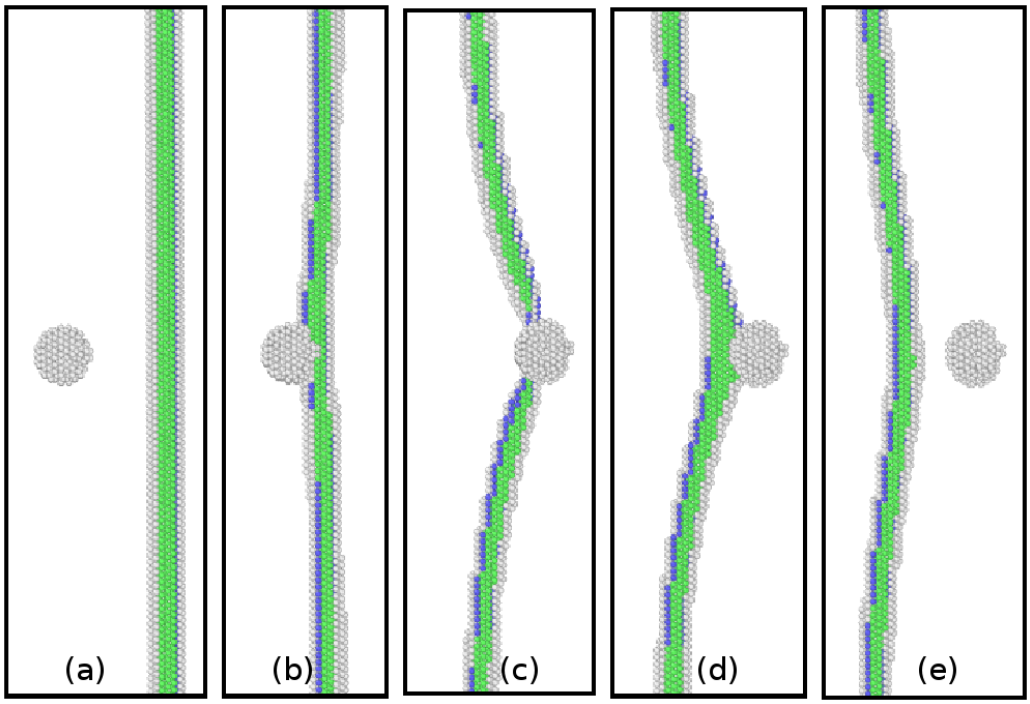

Figure 4: Progressive shearing of a $Mg_{17}Al_{12}$ precipitate of 2 nm in diameter by a screw basal dislocation. The OR was $[0001]_{Mg} \parallel [110]_{\beta}$ and the X axis (horizontal) was parallel to the [111] direction in the precipitate. The Z axis is perpendicular to the figure. Atoms in HCP positions are not shown. Green atoms are in FCC positions while blue atoms are in BCC positions. Precipitate and atoms in unknown positions are grey.

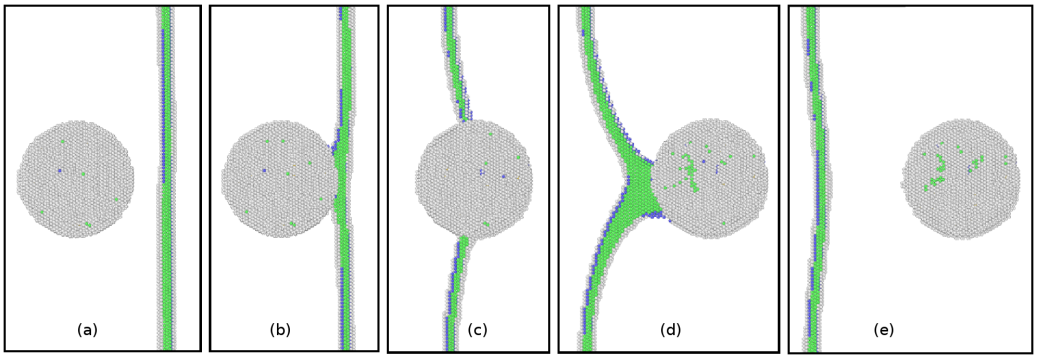

Figure 5: Progressive shearing of a $Mg_{17}Al_{12}$ precipitate of 8 nm in diameter by a screw basal dislocation. The OR was $[0001]_{Mg} \parallel [110]_{\beta}$ and the X axis (horizontal) was parallel to the [111] direction in the precipitate. The Z axis is perpendicular to the figure. Atoms in HCP positions are not shown. Green atoms are in FCC positions while blue atoms are in BCC positions. Precipitate and atoms in unknown positions are grey.

dicted several plausible slip systems, which include [110]/(110), [001]/(110), [110]/(111), and $[1\bar{1}2](111)$ [47]. They are compatible with our observations for the shearing of the precipitates with basal dislocations.

It should also be noticed that shearing of the precipitate along Al-terminated planes was also observed in particular orientations for edge dislocations in precipitates with OR $[0001]_{Mg} \parallel [110]_{\beta}$ (Fig. 7). Shearing the precipitate along the Al-terminated plane was accompanied by the formation of two small jogs in the dislocation with a height of two atomic spacings. Nevertheless, the CRSS necessary to shear the precipitate (which will be reported below) was not influenced by the different shear plane and the presence of the jogs.

Once the dislocation overcomes the precipitate and exits from one side, it re-appears from the opposite side of the simulation box due to periodic boundary conditions along the dislocation glide direction. Taking advantage of the periodicity, simulations in which the precipitate was sheared by several successive dislocations were carried out to ascertain any changes in the deformation mechanisms. The dislocate/precipitate interaction mechanisms can be observed in Fig. 8, which shows several cross-sections perpendicular to the Y axis through the middle of the precipitate. They show the distribution of the Al and Mg atoms in the precipitate and in the matrix just

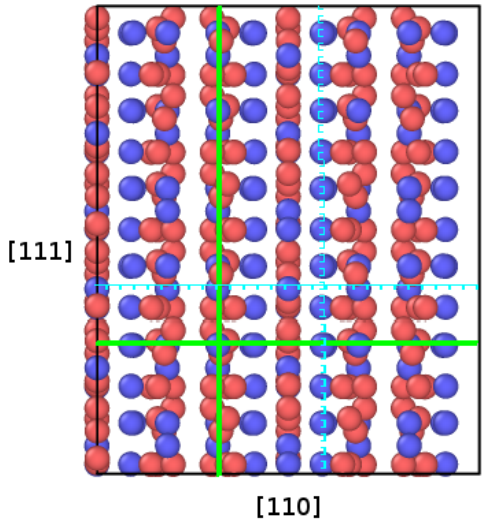

Figure 6: Supercell of the $Mg_{17}Al_{12}$ precipitate. The vertical and horizontal directions correspond to the [111] and [110] orientations, respectively. {111} and {110} planes made up of both Al and Mg atoms are marked in light green while those made up of Al atom are marked in light blue. Al atoms are blue, Mg atoms are red.

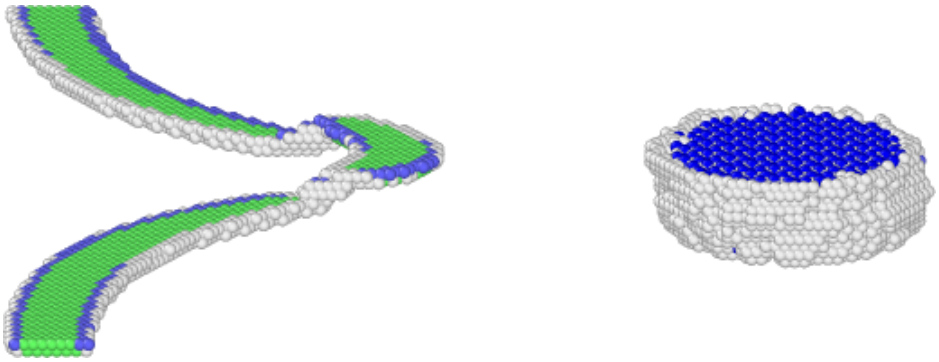

Figure 7: Shearing of the precipitate with OR $[0001]_{Mg} \parallel [110]_{\beta}$ by an edge dislocation along an Al-terminated (110). The (110) plane of the precipitate through which the dislocation shears the precipitate is formed by Al atoms in blue. The formation of two jogs in the dislocation with a height of two atomic spacings is observed in this case, where blue, green, and white atoms represent the BCC, FCC and unknown-structured Mg atoms. The precipitate diameter was 8 nm and the [110] orientation of the precipitate was parallel to the X axis of the simulation box.

before an edge dislocation has entered or exited the precipitate. Successive shearing of the precipitate always took place through the same plane containing Al and Mg atoms, leading to the formation of multiple steps along the matrix/precipitate interface. A step is formed as the first dislocation enters the precipitate from the right (Fig. 8a) and another step appears on the left interface once the dislocation exits from the left (Fig. 8b). More steps at the interface are created as the dislocation enters and exits the precipitate the second time (Figs. 8c and d) and the third time (Figs. 8e and f). In addition, voids due to matrix/interface debonding develop to accommodate the differences in the plastic shearing of the matrix and the precipitate.

4.2. Mechanics

The atomistic simulations also provide the shear stress- shear strain curve during the deformation of the periodic simulation cell. Figs. 4.2a and b show the mechanical response when precipitates of 2 nm and 8 nm of diameter with OR $[0001]_{Mg} \parallel [110]_{\beta}$ are sheared by edge and screw dislocations, respectively. They correspond with Figs. 2, 3, 4 and 5, which depict the evolution of the dislocation/precipitate interaction with the applied load. The initial region of the curves is linear and the slope is given by the shear modulus, $\mu = 12.8$ GPa, according to this atomic potential [38], which is lower than the actual shear modulus of Mg (≈ 16.4 GPa). A certain non-linearity in the stress-strain curves is observed afterwards in the case of the edge dislocations, that corresponds to the shearing of the precipitate for the LP and TP dislocations (Figs. 2b and 3b) and the CRSS is attained once the TP overcomes the precipitate (Figs. 2d and 3d). Afterwards, the shear stress decreases as the dislocation exits the simulation and the whole process is repeated. The curves corresponding to the screw dislocation are equivalent although the non-linear region during the shearing the precipitate is missing and the CRSS is higher than that for edge dislocations for the same precipitate diameter.

The CRSSs, τ_c, for edge and screw dislocations in the presence of β precipitates with OR $[0001]_{Mg} \parallel [110]_{\beta}$ are plotted as a function of the precipitate diameter in Fig. 10. These CRSSs were obtained when the [111] direction of the precipitate was parallel to the X axis of the simulation box but similar values were obtained when the X axis was parallel to the [110] direction of the precipitate. As expected, τ_c increased with the precipitate diameter and the stress necessary to overcome the precipitate was higher for screw dislocations. As no differences were found in the precipitate shear mechanisms

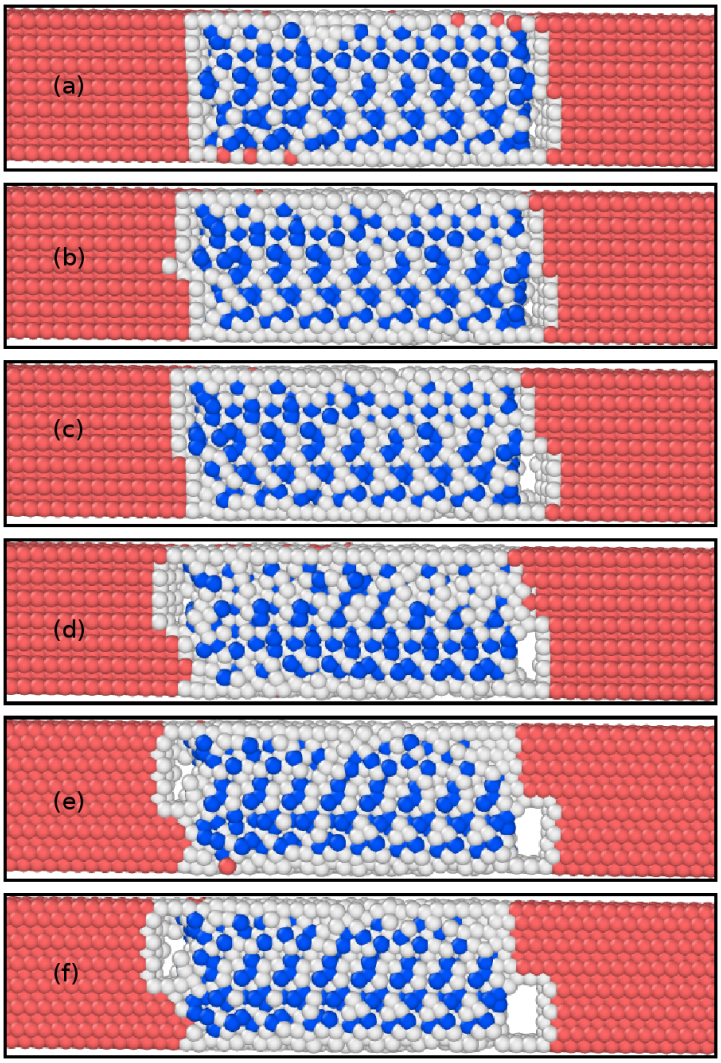

Figure 8: Cross-sections through the middle of a $Mg_{17}Al_{12}$ precipitate of 8 nm in diameter with OR was $[0001]_{Mg} \parallel [110]_{\beta}$. The precipitate is successively sheared by edge basal dislocations. (a) After the first dislocation enters the precipitate from the right. (b) After the first dislocation exits the precipitate from the left. (c) After the second dislocation enters the precipitate. (d) After the second dislocation exits the precipitate. (e) After the third dislocation enters the precipitate. (f) After the third dislocation exits the precipitate. Red atoms stand for Mg in the matrix, grey atoms for Mg in the precipitate and Al atoms are blue. Matrix-precipitate debonding is also observed after the second dislocation shears the precipitate.

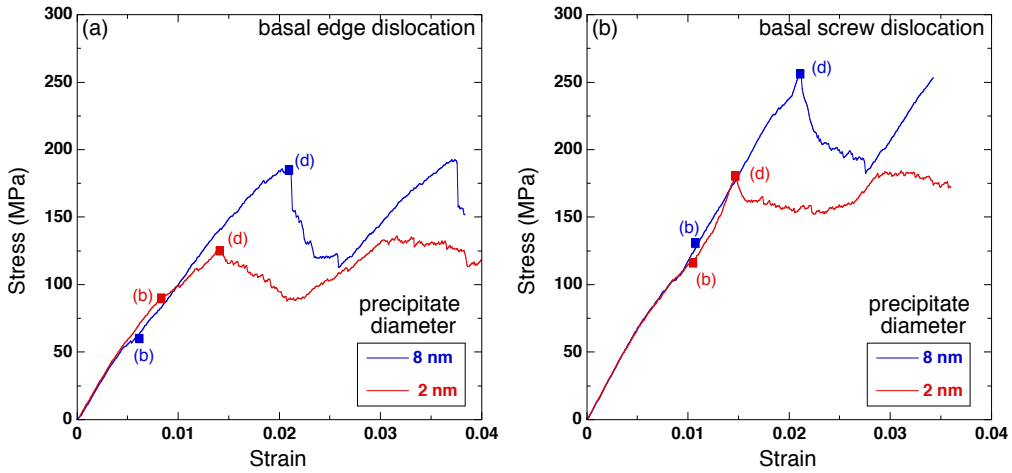

Figure 9: Shear stress - shear strain curves from molecular statics simulations. (a) Edge dislocation. (b) Screw dislocation. The OR of the precipitates was $[0001]_{Mg} \parallel [110]_{\beta}$. The letters in the stress-strain curves correspond to instants of the dislocation/precipitate interaction depicted in Figs. 2b and d, Figs. 3b and d, Figs. 4b and d, and Figs. 5b and d.

between edge and screw dislocations, the mismatch in τ_c is not obvious, but it cannot be attributed to the the Peierls stress of screw dislocations (16 MPa) which was very similar to that of edge dislocations ($\approx$ 11 MPa).

Although the precipitates were sheared by the dislocations and no Orowan loops were formed, it is interesting to compare τ_c with the Orowan stress, $\tau_O = \mu b/L = 123$ MPa where $b = 0.32$ nm is the Burgers vector, $L = 33$ nm the width of the periodic simulation cell and $\mu = 12.8$ GPa the shear modulus coming from atomistic simulations. Although it can be argued that the actual shear modulus of Mg is higher ($\approx$ 16.4 GPa) (and, thus, τ_O could reach 158 MPa), it was decided to use the shear modulus of the atomistic simulations to compute the Orowan stress for consistency. In any case, the CRSS was higher than the Orowan stress for most precipitate diameters but Orowan loops were never found.

The CRSSs, τ_c, for edge and screw dislocations in β precipitates with OR $[0001]_{Mg} \parallel [111]_{\beta}$ are plotted as a function of the precipitate diameter in Fig. 11. As in the previous case, these results were obtained for precipitates in which the X axis of the simulation cell is parallel to the [110] direction of

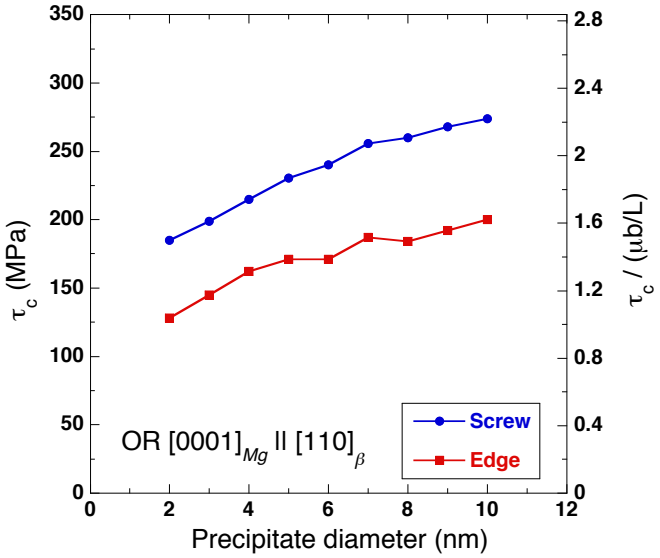

Figure 10: Evolution of the critical resolved shear stress, τ_c, as a function of the precipitate diameter for precipitates with OR $[0001]_{Mg} \parallel [110]_{\beta}$.

the precipitate but they were equivalent to those found when the X axis was parallel to the [112] direction. The evolution of τ_c with precipitate size in Fig. 11 was very similar to that reported in Fig. 10 for β precipitates with OR $[0001]_{Mg} \parallel [110]_{\beta}$. In the case of small precipitates (diameter < 6 nm), τ_c was independent of the OR. However, τ_c was slightly higher for a given precipitate diameter and dislocation character in the [111] orientation than in the [110] orientation and the differences were larger in the case of screw dislocations. These differences cannot be attributed to a change in mechanism but to the stress necessary to shear the precipitate. Atomistic simulations of the generalized stacking fault energy in β-$Mg_{17}Al_{12}$ precipitates [47] found that the energies corresponding to the [001](110) and [110](110) slips systems were lower than those computed for [110](111) and $[1\bar{1}2](111)$ slip systems and these differences are in agreement with our molecular statics simulations. However, it should be noted that the actual plastic deformation mechanisms of the $Mg_{17}Al_{12}$ precipitate are difficult to ascertain.

Finally, the evolution of τ_c after successive shearing of the precipitates by edge dislocations was studied and the results are plotted in Figs. 12a and b for precipitates with both ORs. The data for screw dislocations are similar

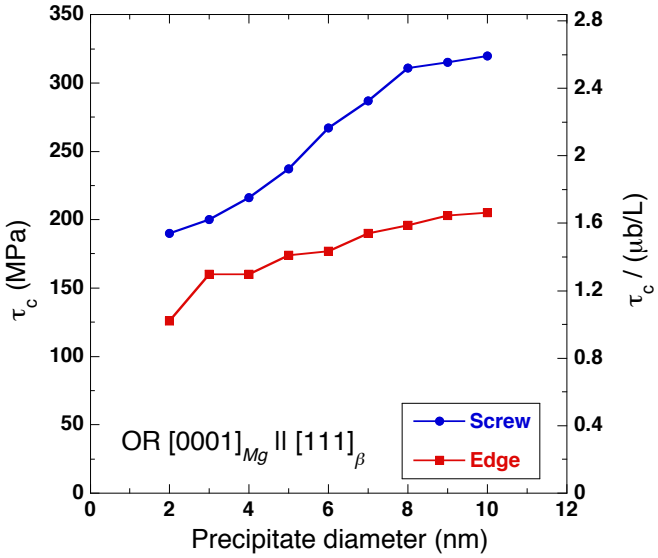

Figure 11: Evolution of the critical resolved shear stress, τ_c, as a function of the precipitate diameter for precipitates with OR $[0001]_{Mg} \parallel [111]_{\beta}$.

and were not included for sake of brevity. These results show that multiple cutting of precipitates by the dislocations did not change the CRSS.

The molecular statics simulations presented above show that $Mg_{17}Al_{12}$ precipitates are sheared by basal dislocations in both ORs. Although the maximum precipitate size studied was rather small (10 nm in diameter), it should be noted that similar simulations carried out in Guinier-Preston (GP) zones as well as θ'' precipitates in Al-Cu alloys showed different mechanisms [19, 48]. Shearing of the GP zones was only found for very small ones (< 3 nm in diameter) when the Burgers vector formed an angle of 60° with the GP plane. Larger GP zones or θ'' precipitates were overcome by the formation of a full Orowan loop or by the LP shearing the GP zone while the TP formed a loop. In the case of screw dislocations, cross-slip of the dislocation to surpass the obstacle was also observed but full shearing was never observed. Thus, our atomistic simulations point out that $Mg_{17}Al_{12}$ precipitates in Mg-Al alloys are more easily sheared by dislocations than θ'' precipitates in Al-Cu alloys. One important consequence of this change in the mechanism is that successive shearing of the precipitates (necessary to maintain plastic flow during deformation) can be achieved in Mg-Al alloys

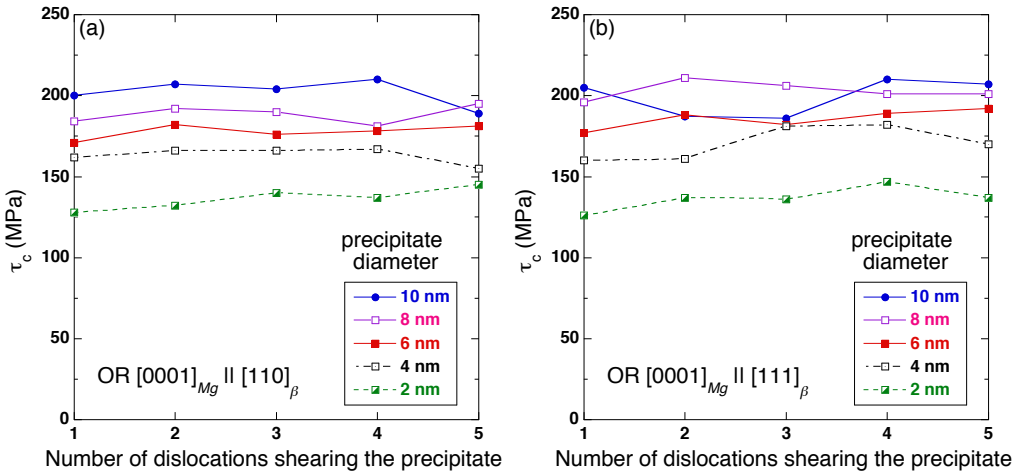

Figure 12: Evolution of the critical resolver shear stress, τ_c, when the precipitate is successively sheared by edge dislocations. (a) Precipitate OR $[0001]_{Mg} \parallel [110]_\beta$. (b) Precipitate OR $[0001]_{Mg} \parallel [111]_\beta$.

at a constant stress. However, the interaction of the successive dislocations with the Orowan loops that have formed around the precipitate leads to an effective increase in the precipitate diameter and to a strong hardening effect in the case of Al-Cu alloys [49].

The molecular static simulations also showed that slightly higher stresses are required for shearing precipitates with OR $[0001]_{Mg} \parallel [111]_\beta$, as compared with OR $[0001]_{Mg} \parallel [110]_\beta$. Nevertheless, the differences were not very large (although they increased with the precipitate diameter) and the results of our simulations seem to agree with the continuum models in the literature which attribute a higher strengthening potential to precipitates elongated along the c axis with OR $[0001]_{Mg} \parallel [111]_\beta$ because they intersect a larger number of basal planes for a given precipitate volume fraction [9, 13].

4.3. Free energy barrier

Molecular dynamics simulations were carried using an NPT ensemble to ascertain the influence of the temperature on the shearing mechanisms and also to gain insights on the energy barriers associated with this process. The simulation boxes were identical to the one used for the molecular statics analyses and contained an edge or screw dislocation and a disc-shaped pre-

cipitate of 8 nm in diameter and 3 nm in height. Simulations were carried out at 150K and 350K for precipitates with OR $[0001]_{Mg} \parallel [110]_{\beta}$ and for precipitates with OR $[0001]_{Mg} \parallel [111]_{\beta}$. In each simulation, a constant shear stress was applied and the time necessary for the dislocation to overcome the precipitate was determined.

The dislocations always sheared the precipitates in the molecular dynamics simulations following the patterns reported above, regardless of the stress and temperature. Thus, precipitate shearing by dislocations seems to be the dominant mechanism in Mg alloys at ambient temperature in agreement with the experimental observations [14]. Another interesting result of the molecular dynamics simulations is the time t necessary to overcome the precipitate. According to the transition state theory, the rate $r = (1/t)$ at which an ergodic system overcomes an obstacle is given by [50]

$$r = \bar{\nu} \exp\left(\frac{-\Delta F}{k_B T}\right) \tag{2}$$

where $\bar{\nu}$ is the frequency factor (of the order of $\approx 10^{11}$ s^{-1} for this kind of barriers [51, 52]), k_B the Bolztmann constant and ΔF the free energy barrier which depends on the stress and temperature and can be expressed as [50]

$$\Delta F = \Delta U(\tau, T) - T\Delta S(\tau, T) \tag{3}$$

where ΔU and ΔS stand for the activation internal energy and the activation entropy, respectively. The activation free energy, ΔF, decreases with both the applied stress and temperature because the applied stress reduces the thermal energy that has to be supplied to overcome the obstacle while the (negative) entropic contribution increases with temperature. While the entropic contribution is not easy to determine, the dependence of ΔF with the applied stress for a periodic array of obstacles has been described by the phenomenological Friedel's model [53]

$$\Delta F = \Delta F_0 \left(1 - \frac{\tau}{\tau_c}\right)^{2/3} \tag{4}$$

where ΔF_0 is the activation free energy at 0 stress and τ_c the CRSS at 0K.

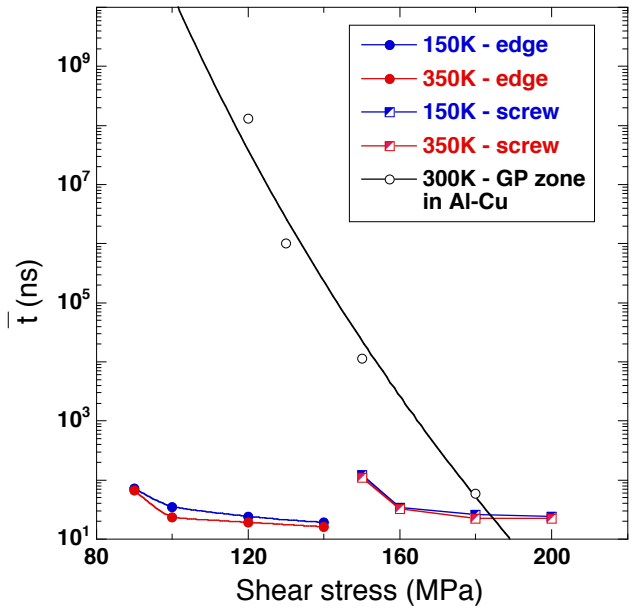

Figure 13: Kinetics of the dislocation/precipitate interaction expressed in the average time $\bar{t}$ (in ns) necessary to shear the β precipitate of 8 nm in diameter with OR $[0001]_{Mg} \parallel [110]_{\beta}$ as a function of the applied shear stress and temperature. The open black symbols stands for the results in [51] corresponding to the interaction of an edge dislocation with a Guinier-Preston zone on the (100) plane in an Al-Cu alloy at 300K are also shown for comparison. The solid black line stands for the fitting of eq. (4) to these results. See text for details.

The time t to overcome a precipitate was computed using molecular dynamics simulations at 150K and 350K as a function of the applied shear stress and the average time $\bar{t}$ (obtained from several simulations in each condition) is plotted in Fig. 13 for edge and screw dislocations and precipitates with OR $[0001]_{Mg} \parallel [110]_{\beta}$. The results for the OR $[0001]_{Mg} \parallel [111]_{\beta}$ are very close and are not included for the sake of clarity. In addition, the predictions of $\bar{t}$ obtained by Saroukhani *et al.* [51] using the transition interface sampling method [54] are plotted in this figure for an edge dislocation and a Guinier-Preston zone in an Al-Cu alloy. The black solid lines stands for the fitting of Al-Cu data with eq. (4) with $\tau_c = 300$ MPa (obtained from molecular statics simulations), which leads to $\Delta F_0 = 1.7$ eV in the case of Al-Cu alloys strengthened by Guinier-Preston zones

The molecular dynamics simulations in the Mg-Al alloy cannot cover the

range of times provided by the transition interface sampling method but – even if the range of times and stresses explored is limited – they show very large differences with the behaviour found in Al-Cu alloy. In particular, the CRSSs in the athermal limit were large (184 MPa and 260 MPa for edge and screw dislocations when the precipitate diameter was 8 nm, Fig. 10). However, the activation free energy is very small and the precipitates are easily sheared by dislocations at much lower stresses at 150K and 350K (90 MPa and 150 MPa for edge and screw dislocations, respectively) because thermal activation provides the necessary energy. This behavior is very different from the one observed in Al-Cu where the energy barrier is large and much larger stresses have to be applied for overcome the precipitates at 300K. In addition, molecular dynamics simulations of the interaction of basal dislocations with β precipitates show that the stress necessary to shear the precipitates in the presence of thermal activation is lower than the theoretical Orowan stress and provides an explanation for prevalence of precipitate shearing with respect to the formation of loops around the precipitates in Mg alloys, in agreement with experimental observations [14].

5. Conclusions

The interaction between $< a >$ edge and screw basal dislocations in Mg and β-$Mg_{17}Al_{12}$ precipitates was studied using atomistic simulations. The mechanisms of dislocation/precipitate interaction as well as the CRSS were analyzed for precipitates from 2 nm to 10 nm in diameter with two different orientation relationships ($[0001]_{Mg} \parallel [110]_{\beta}$ and $[0001]_{Mg} \parallel [111]_{\beta}$). Precipitates were always sheared by the precipitates along {110} and {111} planes, depending of the orientation, and no differences in the mechanisms were found when the precipitates were sheared by either edge or screw dislocations or between 0K and 350K. Successive shearing of the precipitates by dislocations led to the formation of voids at the matrix/precipitate interface.

The CRSS at 0K increased with the precipitate size and it was always higher in the case of screw dislocations. No large differences were found in the CRSS necessary to overcome precipitates with OR $[0001]_{Mg} \parallel [110]_{\beta}$ or OR $[0001]_{Mg} \parallel [111]_{\beta}$. Successive shearing of the precipitates did not change the CRSS. Although the CRSS at 0K was higher than the theoretical Orowan stress, molecular dynamics simulations showed that the activation free energy associated with the shearing of β-$Mg_{17}Al_{12}$ precipitates was very

low, and thus, the actual stress necessary to shear the precipitates decreased rapidly in the presence of thermal activation.

All together, these atomistic simulations provide new insights in the limited strengthening provided by β- $Mg_{17}Al_{12}$ precipitates in Mg-Al alloys that cannot only be attributed to an orientation effect as most β precipitates grow with an habit plane parallel to the basal plane. The easy shearing of the precipitates by the dislocations and the small activation free energy for precipitate shearing also seem to play an important role and suggest that other intermetallic compounds should be included in the microstructure to improve the mechanical performance.

6. Acknowledgments

This investigation was supported by the European Research Council under the European Unions Horizon 2020 research and innovation programme (Advanced Grant VIRMETAL, grant agreement No. 669141). AM acknowledges the Marie Curie fellowship from the AMAROUT-II program. In addition, the computer resources and the technical assistance provided by the Centro de Supercomputación y Visualización de Madrid (CeSViMa) are gratefully acknowledged.

References

[1] A. Kelly, R. B. Nicholson, Precipitation hardening, Progress in Materials Science 10 (1963) 151–191.

[2] C. Varvenne, G. P. M. Leyson, M. Ghazisaeidi, W. A. Curtin, Solute strengthening in random alloys, Acta Materialia 124 (2017) 660–683.

[3] J. F. Nie, Precipitation and hardening in magnesium alloy, Metallurgical and Materials Transactions 43A (2012) 3891–3939.

[4] J. B. Clark, Age hardening in a Mg-9 wt.% Al alloy, Acta Metallurgica 16 (1968) 141–152.

[5] M. A. Gharghouri, G. C. Weatherly, J. D. Embury, The interaction of twins and precipitates in a mg-7.7at% al alloy, Philosophical Magazine 78 (1998) 1137–1149.

[6] N. Stanford, J. Geng, Y. B. Chun, C. H. J. Davies, J. F. Nie, M. R. Barnett, Effect of plate shaped particle distributions on the deformation behaviour of magnesium alloy AZ91 in tension and compression, Acta Materialia 60 (2012) 218–228.

[7] W. B. Hutchinson, M. R. Barnett, Effective values of critical resolved shear stress for slip in polycrystalline magnesium and other HCP metals, Scripta Materialia 63 (2010) 737–740.

[8] V. Herrera-Solaz, J. LLorca, E. Dogan, I. Karaman, J. Segurado, An inverse optimization strategy to determine single crystal mechanical behavior from polycrystal tests: Application to AZ31 Mg alloy, International Journal of Plasticity 57 (2014) 1 – 15.

[9] C. R. Hutchinson, J. F. Nie, S. Gorsse, Modeling the precipitation processes and strengthening mechanisms in a Mg-Al-(Zn) AZ91 alloy, Metallurgical and Materials Transactions 36A (2005) 2093–2105.

[10] V. Herrera-Solaz, P. Hidalgo-Manrique, M. T. Pérez-Prado, D. Letzig, J. LLorca, J. Segurado, Effect of rare earth additions on the critical resolved shear stresses of magnesium alloys, Materials Letters 128 (2014) 199 – 203.

[11] S. R. Rada, P. A. Lynch, J. A. Kimpton, M. R. Barnett, In situ x-ray diffraction studies of slip and twinning in the presence of precipitates in AZ91 alloy, Acta Materialia 119 (2016) 145–156.

[12] P. Hidalgo-Manrique, J. D. Robson, M. T. Pérez-Prado, Precipitation strengthening and reversed yield strength asymmetry in Mg alloys containing rare-earth elements: a quantitative study, Acta Materialia 124 (2017) 456–467.

[13] J. F. Nie, Effect of precipitate shape and orientation on dispersion strengthening in magnesium alloy, Scripta Materialia 48 (2003) 1009–1015.

[14] J. Wang, N. Stanford, Investigation of precipitate hardening of slip and twinning in Mg5%Zn by micropillar compression, Acta Materialia 100 (2015) 53–63.

[15] Y. Xiang, D. J. Srolovitz, L.-T. Cheng, E. Weinan, Level set simulations of dislocation-particle bypass mechanisms, Acta Materialia 52 (2004) 1745–1760.

[16] A. Lehtinen, F. Granberg, L. Laurson, K. Nordlund, M. J. Alava, Multi-scale modeling of dislocation-precipitate interactions in Fe: from molecular dynamics to discrete dislocations, Physical Review E 93 (2016) 013309.

[17] A. M. Hussein, S. L. Rao, M. D. Uchic, T. A. Parthasarathy, J. A. El-Awady, The strength and dislocation microstructure evolution in superalloy microcrystals, Journal of the Mechanics and Physics of Solids 99 (2017) 146–162.

[18] S. Y. Hu, S. Schmauder, L. Q. Chen, Atomistic simulations of interactions between Cu precipitates and an edge dislocation in a B.C.C. Fe single crystal, Physica Status Solidi (b) 220 (2000) 845–856.

[19] C. V. Singh, D. H. Warner, Mechanisms of Guinier-Preston zone hardening in the athermal limit, Acta Materialia 58 (2010) 5797–5805.

[20] G. Bonny, D. Terentyev, L. Malerba, Interaction of screw and edge dislocations with cromium precipitates in ferritic iron: an atomistic study, Journal of Nuclear Materials 416 (2011) 70–74.

[21] M. Liao, B. Li, M. F. Horstemeyer, Interaction between basal slip and a $Mg_{17}Al_{12}$ precipitate in Magnesium, Metallurgical and Materials Transactions 45A (2014) 3661–3669.

[22] M. Bamberger, G. Dehm, Trends in the development of new Mg alloys, Annual Review of Materials Research 38 (2008) 505–503.

[23] S. Celotto, TEM study of continuous precipitation in Mg-9 wt% Al–1 wt%Zn alloy, Acta Materialia 48 (2000) 1775–1787.

[24] A. Crawley, K. Milliken, Precipitate morphology and orientation relationships in an aged Mg-9% Al-1% Zn-0.3% Mn alloy, Acta Metallurgica 22 (1974) 577–562.

[25] M. X. Zhang, P. M. Kelly, Crystallography of $Mg_{17}Al_{12}$ precipitates in AZ91D alloy, Scripta Materialia 48 (2003) 647–652.

[26] J. F. Nie, Physical metallurgy of light alloys, in: D. Laughlin, K. Hono (Eds.), Physical Metallurgy, 5th Edition, Elsevier, 2014, pp. 2009 – 2156.

[27] J. Wang, N. Li, C. Wang, J. I. Beltran, J. LLorca, Y. Cui, Computational study of atomic mobility in HCP Mg-Al-Zn ternary alloys, CALPHAD: Computer Coupling of Phase Diagrams and Thermochemistry 54 (2016) 134–143.

[28] J. D. Robson, N. Stanford, M. R. Barnett, Effect of precipitate shape on slip and twinning in magnesium alloy, Acta Materialia 59 (2011) 1945–1956.

[29] M. Liao, B. Li, M. F. Horstemeyer, Interaction between prismatic slip and a $mg_{17}al_{12}$ precipitate in magnesium, Computational Materials Science 79 (2013) 534–539.

[30] S. Plimpton, Fast parallel algorithms for short-range molecular dynamics, Journal of Computational Physics 117 (1995) 1 – 19.

[31] X.-Y. Liu, J. B. Adams, F. Ercolessi, J. A. Moriarty, Eam potential for magnesium from quantum mechanical forces, Modelling and Simulation in Materials Science and Engineering 4 (1996) 293–303.

[32] M. I. Mendelev, M. Asta, M. J. Rahman, J. J. Hoyt, Development of interatomic potentials appropriate for simulation of solid-liquid interface properties in Al-Mg alloys, Philosophical Magazine 89 (2009) 3269–3285.

[33] B. Jelinek, S. Groh, M. F. Horstemeyer, J. Houze, S. G. Kim, G. J. Wagner, A. Moitra, M. I. Baskes, Modified embedded atom method potential for Al, Si, Mg, Cu, and Fe alloys, Physical Review B 85 (2012) 245102.

[34] Y.-M. Kim, N. J. Kim, B.-J. Lee, Atomistic modeling of pure Mg and Mg-Al systems, CALPHAD: Computer Coupling of Phase Diagrams and Thermochemistry 33 (2009) 650–657.

[35] H. Tonda, S. Ando, Effect of temperature and shear direction on yield stress by $11\bar{2}2 < \bar{1}\bar{1}23 >$ slip in hcp metals, Metallurgical and Materials Transactions A 33 (2002) 831–836.

[36] B. A. Szajewski, W. C. Curtin, Analysis of spurious image forces in atomistic simulations of dislocations, Modelling and Simulation in Materials Science and Engineering 23 (2015) 025008.

[37] P. Hirel, Atomsk: A tool for manipulating and converting atomic data files, Computer Physics Communications 197 (2015) 212 – 219.

[38] S. Groh, E. B. Martin, M. F. Horstemeyer, D. J. Bammann, Dislocation motion in magnesium: a study by molecular statics and molecular dynamics, Modelling and Simulation in Materials Science and Engineering 17 (2009) 075009.

[39] Y. N. Osetsky, D. J. Bacon, An atomic-level model for studying the dynamics of edge dislocations in metals, Modelling and Simulation in Materials Science and Engineering 11 (2003) 427–446.

[40] J. Marian, W. Cai, V. Bulatov, Dynamic transitions from smooth to rough to twinning in dislocation motion, Nature Materials 3 (2004) 158–163.

[41] J. Chaussidon, M. Fivel, D. Rodney, The glide of screw dislocations in bcc Fe: Atomistic static and dynamic simulations, Acta Materialia 54 (2006) 3407–3416.

[42] M. Parrinello, A. Rahman, Polymorphic transitions in single crystals: A new molecular dynamics method, Journal of Applied Physics 52 (1981) 7182–7190.

[43] M. A. Bhatia, K. N. Solanki, A. Moitra, M. A. Tschopp, Investigating damage evolution at the nanoscale: Molecular dynamics simulations of nanovoid growth in single-crystal aluminum, Metallurgical and Materials Transactions 44A (2013) 617–626.

[44] D. Faken, H. Jónsson, Systematic analysis of local atomic structure combined with 3d computer graphics, Computational Materials Science 2 (1994) 279–286.

[45] H. Tsuzuki, P. S. Branicio, J. P. Rino, Structural characterization of deformed crystals by analysis of common atomic neighborhoods, Computer Physics Communications 177 (2007) 518–523.

[46] A. Stukowski, Visualization and analysis of atomistic simulation data with OVITO - the Open Visualization Tool, Modelling and Simulation in Materials Science and Engineering 18 (2010) 015012.

[47] W. Xiao, X. Zhang, W. T. Geng, G. Lu, Atomistic study of plastic deformation in Mg-Al alloys, Materials Science and Engineering A 586 (2013) 245–252.

[48] C. V. Singh, D. H. Warner, An atomistic-based hierarchical multiscale examination of age hardening in an Al-Cu alloy, Metallurgical and Materials Transactions 44A (2013) 2625–2644.

[49] S. Queyreau, G. Monnet, B. Devincre, Orowan strengthening and forest hardening superposition by dislocation dynamics simulations, Acta Materialia 58 (2010) 5586–5595.

[50] W. Kocks, Thermodynamics and kinetics of slip, Progress in Materials Science 19 (1975) 1 – 291.

[51] S. Saroukhani, L. Nguyen, K. W. K. Leung, C. V. Singh, D. H. Warner, Harnessing atomistic simulations to predict the rate at which dislocations overcome obstacles, Journal of the Mechanics and Physics of Solids 90 (2016) 203 – 214.

[52] S. Saroukhani, D. Warner, Investigating dislocation motion through a field of solutes with atomistic simulations and reaction rate theory, Acta Materialia 128 (2017) 77 – 86.

[53] G. P. M. Leyson, W. A. Curtin, Thermally-activated flow in nominally binary Al-Mg alloys, Scripta Materialia 111 (2016) 85 – 88.

[54] T. S. Van Erp, P. G. Bolhuis, Elaborating transition interface sampling methods, Journal of Computational Physics 205 (2005) 157 – 181.